Neutronic Design and Measured Performance of the Low Energy Neutron Source (LENS) Target Moderator Reflector Assembly

C.M. Lavelle [a,*] D.V. Baxter [a] A. Bogdanov [a] V.P. Derenchuk [a] H. Kaiser [a] M.B. Leuschner [a] M. A. Lone [b] W. Lozowski [a] H. Nann [a] B. v.Przewoski [a] N. Remmes [a] T. Rinckel [a] Y. Shin [a] W.M. Snow [a] P.E. Sokol [a]

[a] *IUCF 2401 Milo B. Sampson Lane, Bloomington, IN 47408*

[b] *1449 W Barstow Ave, Fresno, CA, USA 93711*

Abstract

The Low Energy Neutron Source (LENS) is an accelerator-based pulsed cold neutron facility under construction at the Indiana University Cyclotron Facility (IUCF). The idea behind LENS is to produce pulsed cold neutron beams starting with ∼MeV neutrons from (p,n) reactions in Be which are moderated to meV energies and extracted from a small solid angle for use in neutron instruments which can operate efficiently with relatively broad (∼1 msec) neutron pulse widths. Although the combination of the features and operating parameters of this source is unique at present, the neutronic design possesses several features similar to those envisioned for future neutron facilities such as long-pulsed spallation sources (LPSS) and very cold neutron (VCN) sources. We describe the underlying ideas and design details of the target/moderator/reflector system (TMR) and compare measurements of its brightness, energy spectrum, and emission time distribution under different moderator configurations with MCNP simulations. Brightness measurements using an ambient temperature water moderator agree with MCNP simulations within the 20% accuracy of the measurement. The measured neutron emission time distribution from a solid methane moderator is in agreement with simulation and the cold neutron flux is sufficient for neutron scattering studies of materials. We describe some possible modifications to the existing design which would increase the cold neutron brightness with negligible effect on the emission time distribution. [1]

Key words: neutronics, moderators, neutron sources, MCNP
PACS: 29.25.Dz, 02.70.-c, 28.20.Gd, 29.40.-n

[1] This is a preprint version of an article which has been published in Nuclear Instruments and Methods in Physics Research A 587 (2008) 324-341.
http://dx.doi.org/10.1016/j.nima.2007.12.044

1 Introduction

The Low Energy Neutron Source (LENS) at Indiana University is a pulsed neutron source based on (p,xn) reactions in beryllium for proton energies of 13 MeV or less [1,2]. This relatively small-scale neutron source is designed to provide pulsed cold neutron beams of sufficient intensity to conduct neutron research with relatively low cost and minimal source activation, thereby enabling the extension of pulsed slow neutron research into new environments. The relatively low thermal and radiation loads on the cryogenic neutron moderator in this type of source enable new research on cold neutron moderator materials which may possess higher brightness and/or lower spectral temperatures than those presently used at existing slow neutron sources. Operation at a university, made practical by the minimal activation near the target, also makes LENS a model facility for student education and neutron instrument development. The LENS neutronic design is of broader interest because it possesses several features similar to those envisioned for future neutron facilities such as long-pulsed spallation sources (LPSS) and very cold neutron (VCN) sources. The unique operating regime of LENS also encourages speculation about the possibility for realization of entirely new types of neutron sources. We expect LENS to run at a power level of 8 kW or greater starting in 2008. In the following, we benchmark many of our simulations to 30 kW of proton beam power, which we expect to be the practical upper limit for a source of this basic design, limited primarily by thermal stress in the target.

Although not a spallation source, the LENS source neutronics nevertheless shares many features with proposed long-pulse spallation sources since most of the neutrons initially produced in each source are predominantly in the 1-10 MeV energy range. LENS uses a "coupled" moderator (namely, a moderator whose neutron field is directly correlated in space, time and energy with that in the reflector) to cool the 1-10 MeV source neutrons to form a cold neutron pulse width on the order of 1 msec, which is the natural timescale for moderation of fast neutrons in cold hydrogenous materials to the meV energy regime. Since this timescale is also matched to the macropulse width from MW power GeV energy proton linear accelerators, this so-called LPSS accelerator/moderator combination is an attractive possibility for a future high-powered spallation neutron source of increased brightness [3]. With de-

* Corresponding author.
Email addresses: chlavell@indiana.edu (C.M. Lavelle),
baxterd@indiana.edu (D.V. Baxter).

velopments in progress in neutron optics, neutron chopper technology, and neutron spin echo techniques, a large fraction of slow neutron scattering spectrometers of interest for neutron spectroscopy can be designed to accept the ∼msec-wide neutron pulses from such a source [4,5]. Existing short-pulse spallation neutron sources [6,7,8,9,10] achieve narrower pulse widths on the order of 50-100 μs for ∼5 $\mathring{A}$ neutrons [11] to improve the precision of measurement of neutron energy by time-of-flight techniques. The time distribution of neutrons emerging from the moderator, also called the *emission time distribution*, is then much shorter than the time of flight (TOF) from the moderator to the instrument, resulting in high energy resolution. However this order of magnitude reduction in the neutron pulse width is obtained at the cost of a corresponding order of magnitude reduction in the neutron source brightness through the selective use of neutron absorbers near the cold moderator, called decouplers and poisons [11], which limit the effective volume from which thermalized neutrons may enter the beams supplying neutrons to the instruments.

Significant differences between LENS and a typical spallation source include the comparative inefficiency of (p,xn) reactions ($\sim 10^{-2}$ neutrons/proton compared to $\sim$ 20 neutrons/proton for GeV spallation reactions) and a less demanding need for heavy shielding in the forward direction from the target since the most energetic neutrons at LENS are 1.85 MeV below the $\sim$ 10 MeV proton energy. Due to the short penetration depth of the ∼10 MeV protons into the Be target (on the order of 1 mm), the initial source volume for the MeV neutrons is much smaller than for spallation sources. The LENS target lies on the line extended from the instruments through the moderator. This so-called "slab" geometry is more efficient than the "wing" geometry used in most spallation sources[12,13], but is more prone to fast-neutron-induced backgrounds. There are, however, clear similarities between LENS and the current concepts for a LPSS in the operating parameters that matter most to neutron instrument design, namely proton pulse width, moderator coupling, operation frequency, and neutron emission time distribution.

The LENS neutronic design also possesses some overlap with another related type of neutron source envisioned as a possibility for the future: a very cold neutron (VCN) neutron source [14]. Although sharing several features with the LPSS concept, the motivating idea behind a VCN source is to shift the neutron energy spectrum into the VCN energy regime. The VCN energy regime is loosely defined as a regime below a few meV whose lower limit is defined in practice by the point at which the effects of gravity on neutron trajectories are so great that it is no longer possible to make a recognizable neutron beam for neutron scattering measurements. Since the statistical accuracy in (non-interferometric) neutron spectroscopy is directly proportional to the phase space density of the neutron source and the phase space density of a neutron field in equilibrium with a source at temperature T is proportional to $1/T^2$ [15], there is a clear motivation for lowering the neutron energies if neutron

spectrometers are able to make use of the full phase space density of the beam. Since the neutron index of refraction increases for lower energy neutrons it may be possible to design neutron optical elements and spectrometers that fulfill this condition.

Several details of a possible future VCN neutron source have yet to be worked out, and it is by no means clear that a source with sufficient brightness in the VCN range for neutron scattering research can be built. Nevertheless it is clear on general grounds that such a source would possess several neutronic design elements similar to those found in LENS. In common with LENS-type and LPSS-type sources, a VCN source is envisioned to operate in long-pulsed mode with a coupled moderator. The low temperature of the moderator needed to produce a VCN energy spectrum will require cryogenic elements whose neutronic impact on the target/moderator/reflector (TMR) has also been an important element in the LENS design. The potential need for a VCN moderator to employ nuclei with lower neutron absorption cross sections than hydrogen, such as (partially) deuterated materials, means that the volume of the moderator may need to be larger than a typical hydrogenous moderator, and the sensitivity of the VCN moderator brightness to the relative dimensions of a coupled moderator/reflector arrangement are similar to issues also investigated in the course of the LENS design. Finally, if research on cold neutron moderation discovers materials which can efficiently convert neutrons to the VCN energy range, LENS could operate in the VCN energy regime and act also as a useful test bed for some aspects of higher-power VCN sources and instrumentation.

In this article, we summarize the important features of the design of the TMR at LENS and report measurements of the neutron brightness, energy spectrum, and emission time distribution obtained while running the source at $\sim$100 W power. In Section 2 we outline the selection of materials and other general features of the LENS design, and in Section 3 we describe the computer model used to simulate the source and compare the measured performance to the predictions of that model. The detailed neutron transport analyses described in this paper were carried out using the MCNP series of Monte Carlo transport codes [16]. We finish with a description of possible modifications to the system design (Section 4) that could increase the cold neutron brightness and summarize with some conclusions (Section 5).

Historically, many of the relevant concepts for neutron moderation and transport were developed for nuclear engineering and reactor design in time-independent configurations and have subsequently been adapted to describe time-dependent fields encountered in pulsed neutron sources. In this paper we make use of these concepts and the associated language but we also strive to explain some jargon from this field which may be unfamiliar to physicists. We hope that this work might therefore be useful for a somewhat wider audience of scientists,

including those who may be interested to design and construct their own neutron source. The interested reader can find treatments of neutron moderation theory in Glasstone [17] and in Williams [18]. A general overview of neutron sources is found in Carpenter and Yelon [11], Windsor[12] describes many concepts important for pulsed neutron source design, and an excellent review of modern spallation source neutronic design may be found in Watanabe [13].

2 Neutronics

2.1 Overview of the LENS Design Concept

In brief, the LENS neutron source consists of: 1) a proton LINAC capable of delivering a pulsed beam of 7 or 13 MeV with a 25 mA peak current and adjustable pulse width and frequency, 2) a water-cooled Be target, 3) a room-temperature neutron reflector/moderator, 4) a cryogenic moderator and 5) biological shielding. This paper concentrates mainly on those aspects of the LENS source connected with neutron production and moderation. In this section we present an overview of the source properties and some simple dimensional considerations before proceeding to the more detailed neutronic analysis.

The LENS accelerator is capable of producing beam pulse widths from a few microseconds to more than a millisecond. Details of the proton accelerator energy, current, pulse structure, and proposed upgrade path may be found in [19,20,21]. Initially the facility is using an existing 7 MeV Radio Frequency Quadrupole (RFQ)/Drift Tube Linac (DTL) accelerator [22]. Soon a second DTL section will be added to increase the proton energy to 13 MeV, which will increase the neutron yield per proton from the target by a factor of about 4. The peak current and cooling limitations of this accelerator will limit the operation of LENS to 8 kW initially[21]. The ^{9}Be(p,xn) reaction's relatively soft neutron energy spectrum and low production of gamma-rays per neutron make it feasible to operate LENS at a university with an acceptable level of safety and security, and without extensive remote handling facilities for dealing with activated components. The neutrons produced from (p,xn) reactions in Be are less energetic than at spallation sources. The energies of neutrons produced in these reactions are also below the threshold of many reactions which could cause activation in the target. Since the threshold for the ^{9}Be(p,t)^{9}Be reaction is 13.4 MeV, and we wish to minimize target activation, we have chosen a maximum proton energy of 13 MeV. Gamma production in the target is dominated by the ^{9}Be(p,α)^{6}Li channel, which produces one 3.56 MeV gamma for every ten neutrons liberated from the target [23]. Fission and spallation sources typically generate 5-10 gamma rays per neutron [24,25,26]

directly in the source/target. Neutron capture in the reflector, and not proton reactions in the target, is the dominant source of gammas within the LENS TMR. However, the neutron capture gamma rays are also a more distributed source of radiation than the gamma rays produced in the target. The primary construction materials near the target and moderator are Be and Al, so the long-term gamma field from activated products at the center of the source is dominated by alloying elements in these materials. Thus, we expect the activation of TMR materials have negligible impact on the instrument backgrounds and we expect the radiological hazard even of these core TMR materials to be low enough so as to be manageable without the need remote handling.

It is not difficult to estimate some of the relevant length scales and time scales for the LENS TMR. LENS employs a light-water reflector coupled to a cryogenic methane cold source in a geometry which minimizes neutron absorption without unduly broadening the neutron pulse width. The primary neutrons rapidly slow down to thermal energies in the water reflector through elastic collisions with the protons in the water, and then diffuse throughout the TMR until they leak out or are absorbed. Relevant length scales include (a) the neutron slowing down length, which is the RMS distance from from the point where a fast neutron enters the medium to where its energy is lowered to a fraction of an eV, (b) the diffusion length, which is the distance such a thermalized neutron diffuses before being absorbed, and (c) the migration length, which is the quadrature sum of the neutron slowing down length and the diffusion length. For water, this migration length is on the order of 6 cm, and therefore we expect to need a reflector volume with a radius on the order of 20 cm, or three migration lengths. The cold moderator is fed by the neutrons that thermalize in the reflector, so the emission time distribution of the moderator is strongly correlated to the neutron transport properties of the reflector. Also, since our reflector is large compared to the migration length, the characteristic decay rate for the neutrons is set by the absorption rate of the thermal neutrons in the reflector and is given roughly by [18],

$$\xi = v_{th}\Sigma_a \ [\mathrm{sec}^{-1}] \tag{1}$$

where v_{th} is the thermal neutron velocity and Σ_a is the macroscopic absorption cross-section. Given equation 1, we see that the expected decay time for thermal neutrons in a large water reflector should be about 270 μsec. Table 1 summarizes the various length scales for a number of candidate materials considered for the LENS reflector.

The moderator is cooled to maximize the flux of long wavelength neutrons [27,28,29]. The lower intensity of the fast neutron and gamma fields near the LENS target should allow the LENS moderator to operate at low temperatures without major disruptions from the recombination reactions in the methane [30,31] that have caused problems at spallation sources with operation <20 K.

Table 1
Neutron transport parameters for candidate reflector materials [17]. *Absorption length*: v_{th} times the absorption time; *Diffusion length*: diffusion distance for a thermal neutron in an absorption time; *Slowing down length*: RMS distance from fast-neutron entry point to point at which energy falls below 0.4eV, *Migration length*: thermal diffusion and slowing-down lengths added in quadrature; *Slowing Time*: the average time for a 2 MeV neutron to slow to a 25 meV thermal neutron.

Material	Density (g/cc)	Absorption Length (cm)	Diffusion Length (cm)	Slowing Down Length (cm)	Migration Length (cm)	Slowing Time (μs)
Light Water	1.0	58	2.9	5.7	6.4	10
Heavy Water	1.1	1.25×10^4	100	11	103	67
Beryllium	1.8	770	23.6	9.9	25	46
Graphite	1.6	2780	50.2	19	54	150

Annealing periods for the cold source will need to be determined empirically once the source begins operation at powers in the 10 kW range, but these are expected to be manageable (see also Section 2.3.3 below).

Biological shielding near the source consists of a matrix of lead, borax, polyethylene, and epoxy [32]. A material with high Z is required to attenuate the gamma field produced both in the reflector and by capture gammas from the inner layers of neutron shielding [33]. The first layer of gamma shielding is a high purity lead layer separated from the TMR by a thin flexible boron loaded rubber to reduce the activation of the lead layer [34]. MCNP predicts subsequent layers of alternating borated poly and lead will limit contact dose from neutrons and gammas (at 30 kW power) at the TMR surface to 1 REM/h. The TMR is enclosed within a concrete vault with 1.3 m thick walls, and outside this vault we expect a biological dose rate of less than 1 mREM/h [35].

2.2 Neutron Production Target

The neutrons are produced by bombarding a Be target with protons. A metallic Be target was chosen because of its high neutron yield, high melting point, and mechanical strength. The range of a 13 MeV proton in Be is 1.3 mm and we have chosen a 3 mm thick Be target. The short range of $\sim$ MeV protons in materials also implies the target must be exposed directly to the proton beam vacuum.

Operation of the target at several kW power will induce thermal stresses in the target through mechanical deformation during the proton pulse, time average heating of the target, and the high power density of the incident proton beam. The proton beam will be spread relatively uniformly over an area of $\sim$50 cm^2 on the target by 2 octupole magnets to reduce the peak power density

applied to the target. For higher power operations, the target will be bonded on the back side to an Al substrate cooled with flowing water. The Al plate is designed to employ the concept of hypervapotron cooling [36] to dissipate an average thermal load of up to 30 kW (6 MW/m^2). Hypervaportron cooling achieves high cooling power and avoids possible localized heating of the target from a static vapor layer through proper choice of coolant flow rate, pressure, and channel geometry to set up local circulating flows that sweep bubbles away from the surface. This technique requires only a relatively thin layer of water behind the target. As a result, we have considerable freedom to choose the thickness of water between the target and the moderator to optimize cold neutron production. From the neutronics point of view, this water can act as a premoderator and/or limit the fast neutrons seen by the instruments.

Total neutron yields and energy spectra have been collected from the literature [37,38,39,40] for proton energies up to 23 MeV. An empirical formula for the total neutron yield, Y_N, as a function of the proton energy, E_p in MeV, is [41]

$$Y_N(E_p) = 3.42 \times 10^8 (E_p - 1.87)^{2.05} \text{ [n/}\mu\text{C]}. \quad (2)$$

This gives 1.6×10^{-3} n/p at 7 MeV proton energy and 7.6×10^{-3}n/p at 13 MeV. Normalized energy spectra and angular distributions of the primary neutrons are required as input for modeling with MCNP. Since to our knowledge no experimental data on neutron energy distributions from protons on thick Be targets are available between 5 and 14.8 MeV proton energy, neutron energy distributions were calculated for the incident proton energies of 7 MeV and 13 MeV.

Figure 1 shows measured "thick" target neutron spectral distributions of the ^{9}Be(p,xn) reaction at 0° for the proton energies of 5 MeV [40], 17.2 MeV and 18.4 MeV [39] together with the results of our estimates for 7 and 13 MeV, which will be discussed below. As can be seen, a low energy continuum dominates the spectrum, especially for the higher bombarding energies. The sharp edge at the high-energy end of the neutron spectra corresponds to the kinematic limit of the ^{9}Be(p,n$_o$)^{9}B ground state transition.

Calculations of neutron spectral distributions have to take into account the various reaction mechanisms which contribute to the neutron production. The ^{9}Be(p,n) reaction proceeds through the formation of the compound nucleus, ^{10}B, through direct charge exchange, and through multi-body breakup (^{9}Be is a loosely bound (2α+ n) system which breaks up very easily). Each process contributes to different portions of the neutron spectral distributions. Pre-equilibrium decay of the compound nucleus contributes a high energy tail to the neutron spectra. The multi-body breakup and ^{9}Be(p,p′n) reactions will produce lower energy neutrons with relatively flat angular distributions. The direct charge exchange process generally leads to the production of high energy

neutrons with forward peaked angular distributions. However, its contribution to the total yield decreases steadily with increasing proton energy [42].

Taking into account the general behavior of the various reaction mechanisms which lead to neutron emission, we calculated neutron spectral distributions for a proton bombarding energy of 7 MeV. Excitation functions of angular distributions of differential cross sections of the ^{9}Be(p,n)^{9}B reaction to the ground and first three excited states were calculated with the code DROSG-2000 [43] in 0.1 MeV steps from 7 MeV down to the threshold for θ= 0 to 180° in 20° steps based on data of Young et al. [44]. For each bombarding energy, these differential yields were integrated over solid angle and neutron energy and then subtracted from the total ^{9}Be(p,n) cross section collected by Byrd et al. [42] to give the contributions from the other reaction mechanisms. These other reaction mechanisms of pre-equilibrium compound nucleus decay and multi-body breakup produce nearly isotropic angular distributions. They are described as evaporation spectra, i.e. $\phi(E) \sim Ee^{-E/\tau}$, where E is the neutron energy and τ is an appropriate nuclear temperature. For each angle, these two distributions were combined with equal weight, normalized to the above described difference, and then added to the DROSG-2000 results. After integration over neutron energy and solid angle this sum was normalized to the total neutron yield given in Equation 2.

The neutron spectral distributions for the incident proton energy of 13 MeV were obtained for θ= 0 to 180° in 20° steps by extrapolating the results of Lone et al. [37], measured at bombarding energies of 14.8, 18, and 23 MeV, and Brede et al. [39], measured at 12 energies between 17.2 and 22.0 MeV. This method was considered more accurate than using the above described method for 7 MeV and extrapolating the data of Young et al. [44] to 13 MeV. The normalization to the total neutron yield was done the same way as for 7 MeV.

2.3 Design of Target/Moderator/Reflector (TMR) System

We may define three more-or-less separate neutronic functions for a TMR system: (P) initial production of fast neutrons, (S) slowing down of neutrons from the ∼MeV scale to the ∼eV scale through elastic collisions with light nuclei and delivery to the cold moderator, and (M) moderation of the thermalized neutrons to lower neutron energies through interaction with the inelastic modes of the cold moderator. The information needed for the production (P) step usually either exists with sufficient precision for neutronic purposes or can be interpolated or calculated (as we have been forced to do for (p,n) reactions in Be as described above). Likewise the information needed for step (S) also exists: cross sections are known, and the energy loss per collision in

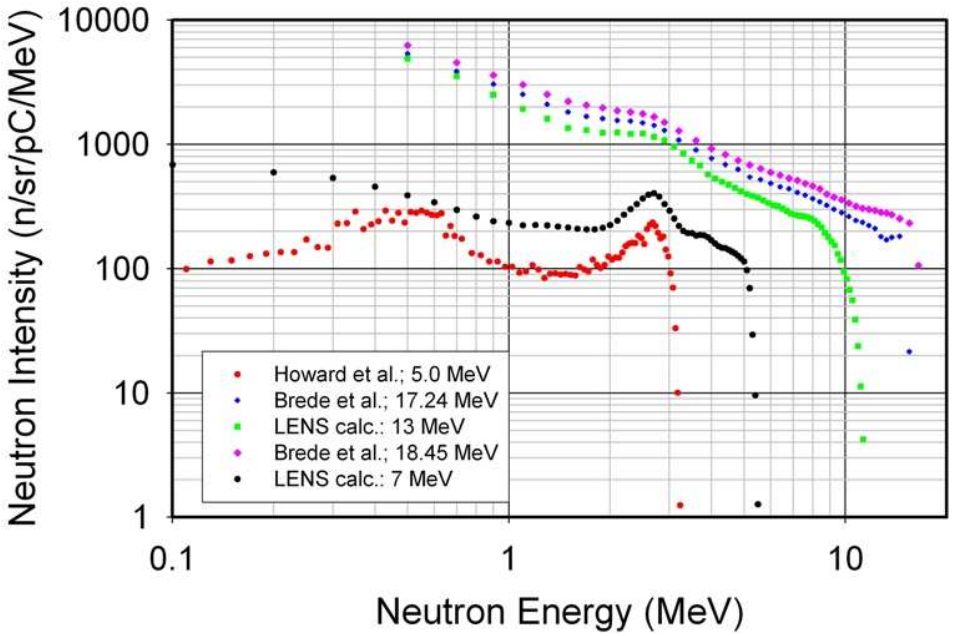

Figure 1. A comparison of measured [40,39] and calculated [41] neutron energy spectra at 0 degrees.

this energy regime can be calculated from elementary classical mechanics. The information needed for step (M) does not always exist since the low energy inelastic mode structures of condensed matter systems depend a great deal on the details of the material's structure, and adequate models are difficult to construct from first principles [45].

It is interesting to note that for various reasons the separation of these three neutronic functions is somewhat more sharply defined for a neutron source of the LENS type than for reactors or spallation sources. Reactor cold neutron sources possess design constraints associated with the need to maintain the fission chain reaction in the reactor, thereby inducing a design coupling between functions (P) and (M). High-power spallation neutron sources are generally designed with several moderators close to the target which compete with the space available for the reflector, thereby effectively introducing a coupling between functions (P) and (S). Both reactors and spallation sources produce the initial fast neutrons in an extended volume, thereby inevitably spatially mixing all three functions, and the intense high energy neutron and gamma fields introduce another coupling of elements (P) and (M) indirectly through the cryogenic demands on the refrigerator for the cold moderator. For a (p,n) reaction source such as LENS, however, these functions can be more cleanly isolated. Due to the $\sim$1 mm range of 10 MeV neutrons in Be, the fast neutrons are emitted from a sharply-defined narrow plane with a transverse area defined by the incident proton beam, thereby spatially isolating function (P). Since neutron beams are extracted from a relatively small solid angle,

the volume of the reflector can be much larger than the volume of the cold moderator, and to the extent that the cold moderator can be viewed as a relatively small perturbation to the neutron field developed by the reflector, a separation of functions (S) and (M) is effected. Finally the lower fast neutron and gamma intensity of the LENS source reduces the heat load on the cryogenic moderator to further weaken the coupling of functions (P) and (M) through cryogenic engineering constraints. The combination of these features simplifies the design process and allows us to separately optimize each of the three components as a starting point for the later refined calculations using realistic geometries.

Since the three main functions noted above possess some independence, we are freer to specify exactly what we want the reflector and the cold moderator to do. In this simplified view, the main purpose of the "reflector" (in reality a combined reflector and moderator) is to moderate the fast neutrons into the thermal energy regime and return the largest possible fraction of them to the cold moderator, and the main responsibility of the cold moderator is to convert these thermalized neutrons as efficiently as possible into the cold neutron regime. Of course, we also note that all this must be done while maintaining a time structure from the combined system such that any long tails present must be acceptably small for the neutron scattering instruments.

The MCNP model geometry of the TMR is shown in Figures 3 and 2. The primary neutronic elements of the source are a cylindrical light water reflector surrounding the beryllium target and a relatively thin solid methane moderator, 12x12x1 cm^3. The mean free path (MFP) of a neutron with energy between a few eV and several keV in solid methane is on the order of 1 cm, and drops to 0.1 cm for thermal neutrons [46,47]. Thus, the methane moderator interacts relatively weakly with the fast neutron field and more strongly with the slow neutron field as required to justify our consideration of reflector and moderator functions separately.

The present TMR design includes extra space around the moderator in order to facilitate experimental studies of various neutronic changes (such as changes in premoderator, moderator geometry, poisons, etc.) at the present very low power levels. We show later in this paper that a gain of a factor of up to 1.3 in neutron moderator brightness at a given proton beam power is possible if this vacuum space is reduced considerably.

2.3.1 Moderator geometry

MCNP calculations using a simplified model of infinite plane slabs of finite thickness 22 K solid methane moderator were performed to determine the dependence of cold neutron brightness on methane thickness using the *smeth22k*

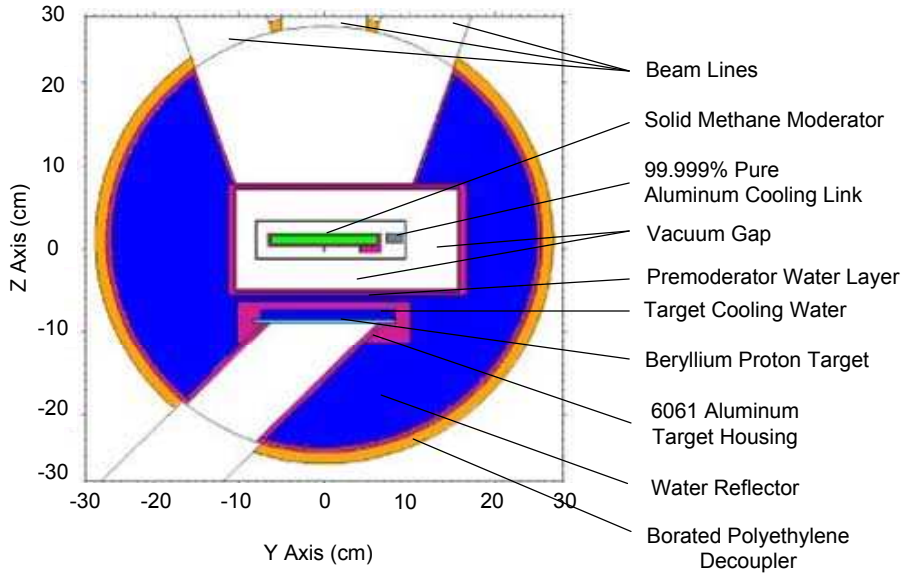

Figure 2. YZ Planar view of the TMR geometry. The 1 cm thick methane moderator is at the center, forward of the target and target cooling. The target and moderator are surrounded by a light water reflector of radius 25 cm, decoupled from the shielding layers by a 5 cm thick borated poly layer. Biological shielding layers are not shown for clarity, but are included in the simulations.

kernel [46]. If cold neutrons are to be produced directly from the primary fast neutron flux with negligible premoderation, as is true with most spallation source designs to date, then the optimal thickness of methane is about 5 cm, as one finds in existing and planned methane moderators at spallation sources such as IPNS and ISIS.

However, we found that if the moderator is designed to couple primarily to the thermal neutron field from the reflector, as in our geometry, then the methane can be thinner, just 1 or 2 cm. This has important consequences for moderator cryogenics: a thinner moderator greatly reduces the heating from fast neutron energy loss in the moderator medium and also reduces the temperature gradient across the thickness of the moderator medium, which possesses poor thermal conductivity at low temperature. Figure 4 shows the relative probability to produce cold neutrons in different energy ranges from a monoenergetic beam of incident neutrons of 100 meV. A broad maximum in cold neutron intensity is observed from 1 to 2 cm methane moderator thickness. To minimize neutron and gamma heating and the thermal gradients, 1 cm was chosen as the thickness of the methane moderator.

More detailed simulations of the emitted cold flux in the full neutronic model using the *smeth22K* kernel confirmed that little cold flux would be gained by going beyond 1 cm thickness and also showed that cold neutrons are emitted

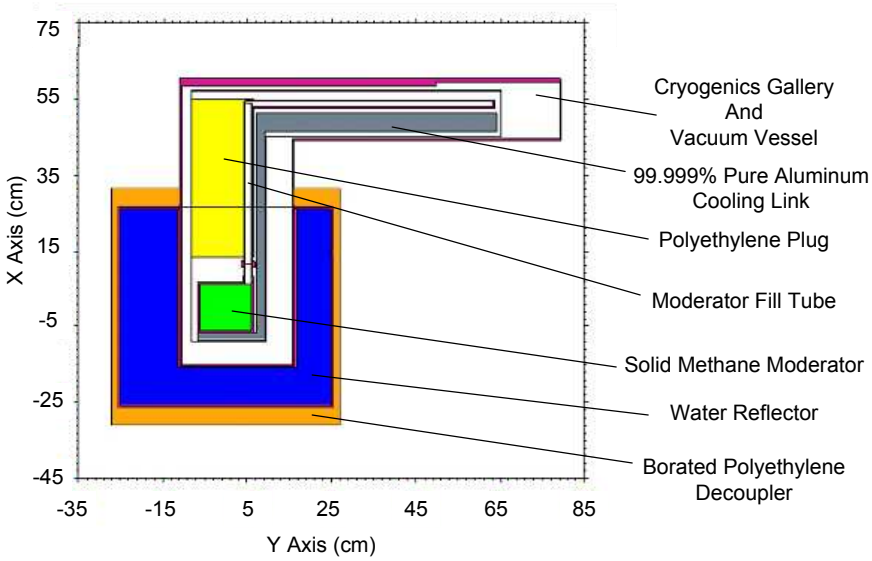

Figure 3. YX Planar view of the TMR geometry. The 12x12 cm methane slab is at the center, connected to the helium refrigerator (not shown) by a 99.999% pure aluminum cold link. The water reflector surrounds the moderator and the polyethylene plug above the moderator provides neutron reflector material inside the cryogenic system. Biological shielding layers are not shown for clarity, but are included in the simulations.

from the moderator surface with a flat spatial distribution for our design. More recent simulations with an improved methane scattering kernel suggest that a thickness of 2 cm may produce a slightly greater cold neutron brightness for methane temperatures less than 20 K [48]. Both MCNP studies confirm the initial insight that the LENS methane moderator can be significantly thinner than found at existing spallation facilities.

Given the size of the neutron beam lines, no more than 10×10 cm^2, it was found that cold neutron flux leaving the moderator's face (the "leakage flux") saturates near $12{\times}12$ cm^2 moderator area and so this size was taken for the lateral dimension of the slab moderator. In order for a neutron to be seen by the instrument, the neutrons incident on the cold moderator must diffuse into a region of the moderator surface viewed by the beam line. The additional width can be understood as the length a low energy neutron from the reflector can travel as it thermalizes in the methane and still contribute to the cold neutron flux. As can be seen in Figure 4, the contribution from thermal neutron energies (>10 meV) falls off rapidly for distances greater than 1.0 cm.

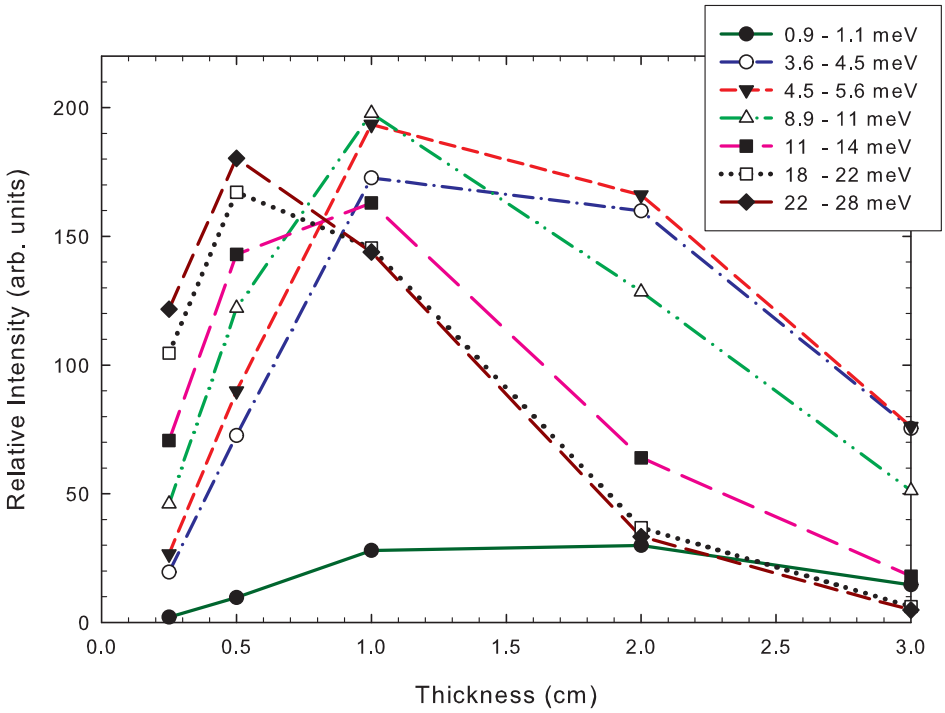

Figure 4. Simulated intensity of cold neutrons emitted from the exit face of an infinite slab, finite thickness methane moderator for a 100 meV pencil neutron beam incident on one side. A broad 1-2 cm maximum is observed for production of cold neutrons .

2.3.2 Reflector material

For a neutron source with strong coupling of the thermal neutron field between the moderator and the reflector, the reflector is actually being employed as both a reflector *and* a thermal neutron source [27,49,50]. Therefore we first considered calculations of reflector materials in model spherical geometries to investigate the ability of various materials to produce high thermal neutron flux in the center of the reflector as a function of primary neutron energy and reflector radius. While many different radii were simulated, a representative result that conveys the general thrust of the calculation is shown in Figure 5. In this figure, 40 cm radius spheres are used with an isotropic point source of fast neutrons at the center. As we have discussed, our design attempts to thermalize the fast neutrons rapidly in the reflector and allow thermal neutrons to diffuse back to the moderator for efficient cold neutron production. For primary neutron energies lower than about 3.5 MeV, light water is the best reflector material. As the primary neutron energy increases above 3.5 MeV, the neutron-hydrogen scattering cross-section decreases, thereby increasing the mean free path and reducing the fraction of thermalized neutrons returned to the moderator. In contrast, for neutron energies above the 3.5 MeV mark (about 25% of the 13 MeV proton source primary yield), Be is

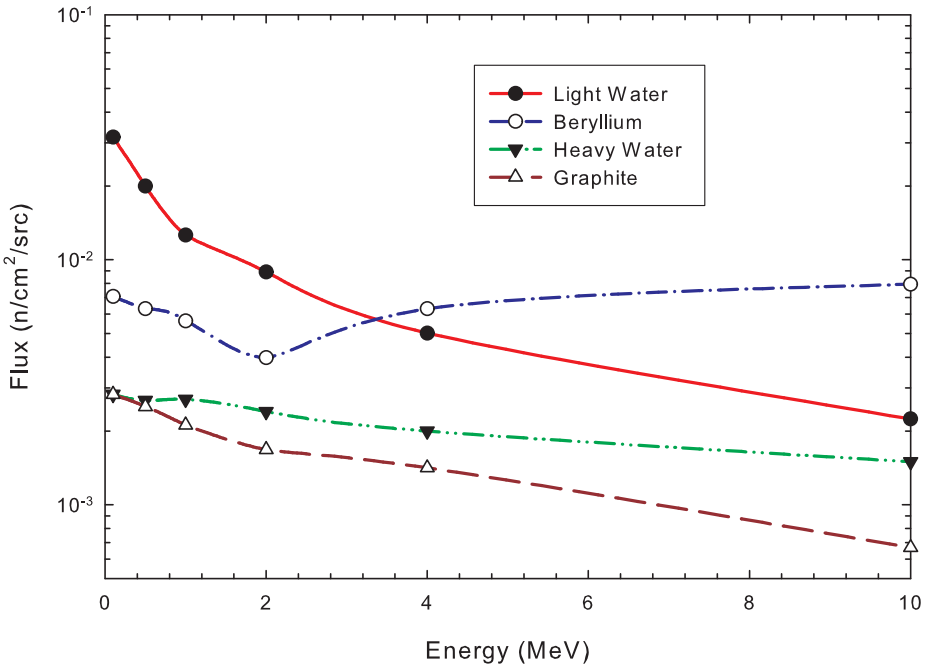

Figure 5. Simulated intensity of thermalized neutron flux per source neutron in the center of spherical ambient temperature reflector materials, radius 40 cm, as a function of the energy of a monoenergetic point source also at the center.

a better reflector for a coupled cold neutron source. This is due to its larger neutron scattering cross section and also the extra neutron production in Be from (n,2n) reactions (which multiplies the primary flux by a factor of 1.09). Although these calculations indicated that Be exhibits better performance, light water was chosen for the initial LENS reflector to minimize both cost and potential activation issues.

We selected a cylindrical reflector of light water 25 cm in radius, 50 cm tall enclosing the production target and moderator based on these simulations. Although no cold flux gain is realized from increasing a water reflector radius beyond 20 cm, calculations indicate that the optimal beryllium reflector radius is 25 cm and we did not want to preclude the possibility of an upgrade to a Be reflector in the future (see Section 4).

2.3.3 Moderator and cryogenics radiation load

The refrigerator that maintains the moderator temperature must remove the heat deposited by fast neutrons and gammas. The gamma rays come from both the production target and from neutron capture on the moderator, reflector, shielding, etc. (see Table 2). We chose a CryoMech PT410 commercial pulse tube mechanical refrigerator [51] to provide the moderator cooling at LENS.

The thermal connection between the moderator vessel and the refrigerator consists of a 99.999% pure Al plate connected to the bottom of the moderator vessel and coupled to the 2^{nd} stage of the refrigerator [52]. The total length of the Al connection is on the order of 1 m in order to take the cold-head far enough away from the source to avoid significant activation of its components. Bench tests with an electrical heater connected to the moderator vessel showed that temperatures below 10 K may be maintained provided that the heat load on the moderator is less than 3 Watts.

Table 2
Neutron and Gamma heat loads on the cryogenic components for 30 kW proton beam power at 13 MeV as calculated in MCNP. There is an additional 180 mW of heating from decay activity in the aluminum components which was calculated separately. An asterisk (*) denotes components that are thermally connected to the (warmer) first stage of the two-stage mechanical refrigerator. All other components are connected to the (colder) second stage.

Cryogenic Element	**Neutron (mW)**	**Capture Photon (mW)**	**Target Photon (mW)**	**Total (mW)**
Solid Methane	420	23	36	**479**
Moderator Vessel	26	83	127	**236**
Fill Tube (lower)	8	20	27	**55**
Fill Tube (upper)	1	6	2	**9**
Aluminum Bar	12	52	44	**108**
Moderator Attachment Flange	1	4	3	**8**
Poly Plug*	267	122	43	**432**
Thermal Shield*	16	72	75	**163**
Total (mW)	**750**	**382**	**357**	***1490***

The thermal load on the various components of the cryogenic system was calculated in MCNP by tallying energy deposition from neutrons and the gamma rays produced both directly in the target and by neutron capture. The contribution to the whole thermal budget from each component is shown in Table 2. A cross-sectional area of 1.8×2.0 cm^2 for the aluminum cooling link produced a total deposited power of 1.5 W into the cryogenics, of which only about 1 W is thermally connected to the second (colder) stage of the refrigerator. Decay gamma and beta heating from activated aluminum is not included in the MCNP calculations, but was estimated from the calculated volume averaged neutron flux in each element to be approximately 180 mW additional power over the course of long term running at full accelerator power. This heat contribution is dominated by ^{28}Al decay in the moderator vessel and thermal link. Since the combined load from these sources is well below the 3 W used in the bench test mentioned above, we are confident that even at 30 kW operation we will be able to keep the moderator at well below 10 K with the existing cryogenic design.

These simulations estimate the specific thermal load on the methane itself

to be only about 3.3 mW/cm^3. At temperatures between 4 and 10 K the thermal conductivity of solid methane is on the order of 10 $\pm$ 5 mW/cm.K [53], so on dimensional grounds we can expect to see gradients on the order of only 0.3-1.0 K/cm through the thickness of the methane even at 30 kW proton power. Therefore the 1 cm thick moderator at LENS will not develop a substantial temperature gradient under foreseen operating conditions. The need for aluminum foam or similar structures used at IPNS to improve thermal contact between the solid methane and the aluminum walls of the moderator vessel therefore disappears [54].

3 Performance - Simulated and Measured

The brightness, flux, emission time distribution, and energy spectrum of neutrons emitted from the moderator are obviously essential parameters for neutron instrument design. The emission time distribution from a long-pulse neutron source such as LENS is broad enough to significantly perturb the normally straight-forward relationship between time-of-flight and neutron energy and so we consider this effect first. Only after understanding the effects of the broad emission time distribution is it possible to perform quantitative comparisons of the brightness, flux and energy spectrum with simulations.

3.1 Emission Time Distributions

3.1.1 Simulation

The emission time distribution is simulated by tallying the neutron leakage flux over the instrument side of the cold moderator face convolved with a square proton pulse as employed in the experiments (150 μs for the results quoted here). A fairly broad cone ($\cos\theta > 0.95$) was accepted in the calculation to enhance Monte Carlo statistics while still retaining sufficient fidelity in representing the conditions of the experimental measurement. This is permissible since the emission time distribution, which for our strongly coupled long-pulse source is dominated by the time-dependent neutron transport properties in the reflector rather than the cold moderator geometry, is a weak function of emission angle across this angular range.

Figure 6 shows the emission time distribution for several low energy neutron groups, and the pulse width (FWHM) is shown in Figure 7 as a function of energy. There is a saturation in the FWHM near 350 μs as the neutrons come into equilibrium with the moderator. The neutron emission rises quickly and subsequently decays over a time period that is consistent with the character-

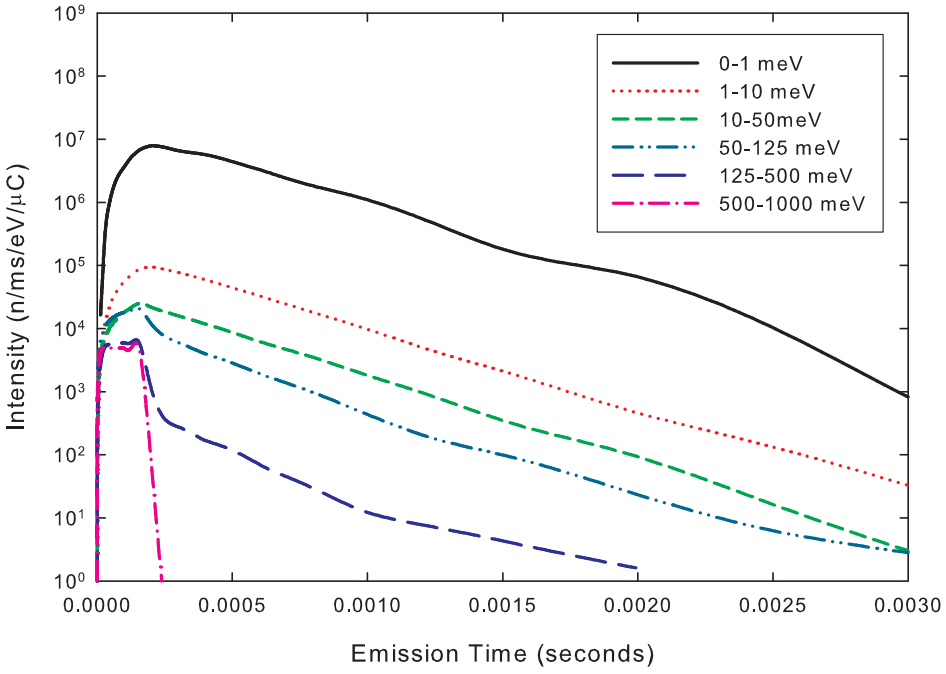

Figure 6. Simulated neutron emission time distributions. The water reflector and coupled 22 K solid methane moderator create long emission times for all low energy neutron groups. The 150 μs proton beam pulse dominates the pulse shapes of higher energy neutrons (500-1000 meV in this figure).

istic decay time in the water reflector. We note that this 350 μsec figure is consistent with the expectations outlined above for a spectrum dominated by a large water reflector/moderator and a 150 μsec proton pulse width.

3.1.2 Measurements

The emission time distribution was measured using a time-focused crystal analyzer spectrometer, which is designed to cancel to first order geometrical effects due to variations in neutron flight path in the plane of the reflection [55,56]. The crystal monochromator employed a Ge mosaic crystal with mosaic width of $\sim \frac{1}{2}$ degree, resulting in an energy resolution of $\sim 3\%$ using the (111) reflection planes. The first order reflection was set for 2.74 meV (5.46 $\mathring{A}$) and the third order reflection was set for 24.6 meV (1.82 $\mathring{A}$); the second order reflection is forbidden. These energies were selected because the first order reflection is near the peak of the cold neutron energy spectrum and the third order reflection is in the thermal neutron range. These neutron energies span the extremes of expected emission time distribution FWHM's shown in Figure 7.

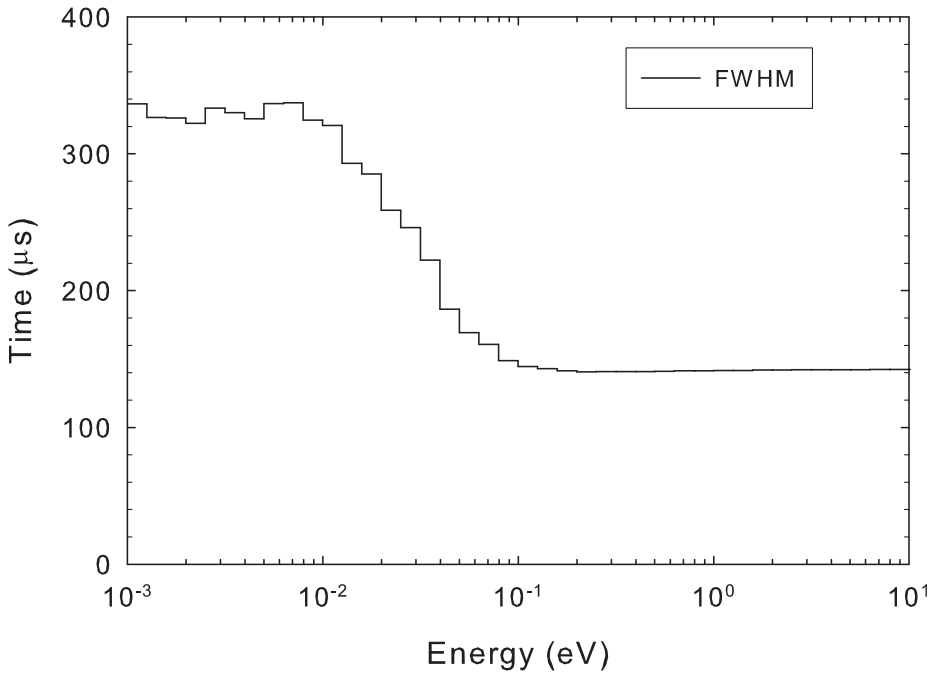

Figure 7. The simulated average emission time FWHM for neutron pulses from a 22 K methane moderator and with a 150 μs proton pulse plotted as a function of neutron energy.

The accelerator parameters for this measurement were a 150 μs square pulse width, a 7 mA peak current, and 15 Hz pulse rate for a time-averaged power of 110 W. The analyzer crystal viewed the moderator through a beam line oriented at 20 degrees off the moderator normal. This particular beam line had a 2-cm aperture at a distance of 135 cm from the moderator and the beam was much larger than the crystal at the analyzer position. Given the broad peaks to be measured, it was not necessary to fine-tune the detector orientation to optimize the time-focussing. We estimate that the instrumental broadening of the measured pulse width is less than 20 μsec. The total flight path was 6.6 meters from the moderator to the detector (moderator to analyzer distance of 6.0 m). The raw data from 12 hours of data collection is shown in Figure 8. The emission time distribution at the energy of the first Bragg peak of 2.74 meV agrees well with MCNP simulation convolved with a 150 μs square proton pulse as shown in Figure 9.

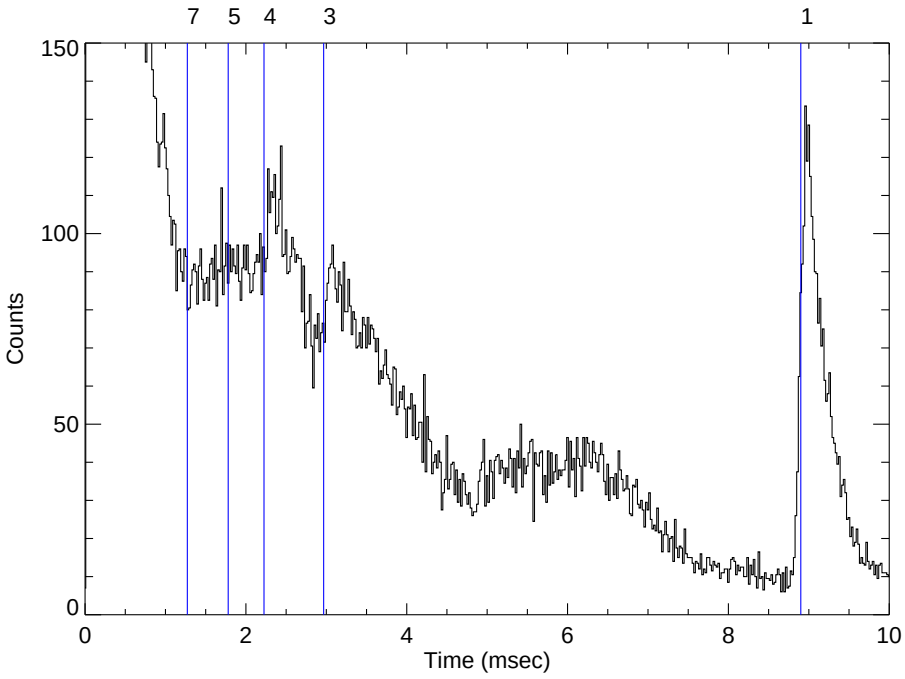

Figure 8. Raw time-of-flight data for Bragg reflections from the (111) reflection planes in a Ge mosaic crystal in a time focussed geometry. The order of reflection is shown at top. Because the energy resolution of the spectrometer is narrow compared to the emission time distribution, the range of energies as reflected in the shape and width of the reflected Bragg peaks gives directly the emission time distribution and FHWM.

3.2 Neutron Energy Spectra

3.2.1 Simulation

Simulated neutron energy spectra (Figure 10) were calculated for a beam line viewing the moderator at 20 degrees from the moderator surface normal. We simulated the energy spectra for three different configurations of the TMR and proton energy: a) 7 MeV proton energy with an empty moderator vessel, b) 7 MeV proton energy with a 22 K methane moderator, and c) 13 MeV proton energy with 22 K methane moderator. Neutron moderation from fast to thermal energies, which occurs through a series of non-relativistic 2-body collisions of a neutron of mass m_n and energy E with a target nucleus of mass A (in units of neutron mass) and energy zero, produce a 1/E neutron energy spectrum in an infinite medium [11]. It is therefore useful to define a quantity, EI(E), called the spectral intensity, that is constant in the epithermal energy range for an infinite medium. The spectral intensity may be related to a measured neutron flux, ϕ(E), through the relation:

$$EI(E) = \frac{L^2}{i} E\phi(E) \tag{3}$$

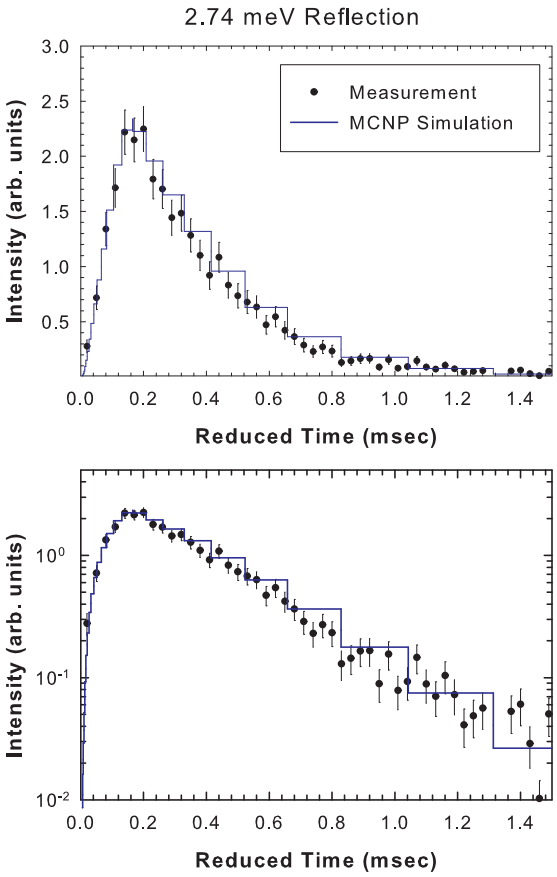

Figure 9. Emission time distribution measurement compared with MCNP simulation convolved with 150 μs square pulse. The time axis is reduced so that each pulse starts at zero time and the integral area is normalized to 1 for both curves.

where E is the neutron energy, $I(E)$ is the luminous intensity in units of $n/sr/\mu C/eV$, L is the flight path length in units of cm, and i is the time averaged proton current. Integral yields, Y in units of $n/sr/\mu C$, are determined from equation 4 for different energy groups and tabulated in Table 3 where they are compared to experimental results.

$$Y = \frac{L^2}{i}\int_a^b \phi(E)dE = \int_a^b I(E)dE \tag{4}$$

3.2.2 TOF Measurement

The standard technique for measuring moderator spectra [57,59] relates the count rate in the detector to the flux through:

$$C(t) = \Delta T A \varepsilon(E)\phi(E)\frac{dE}{dt} \tag{5}$$

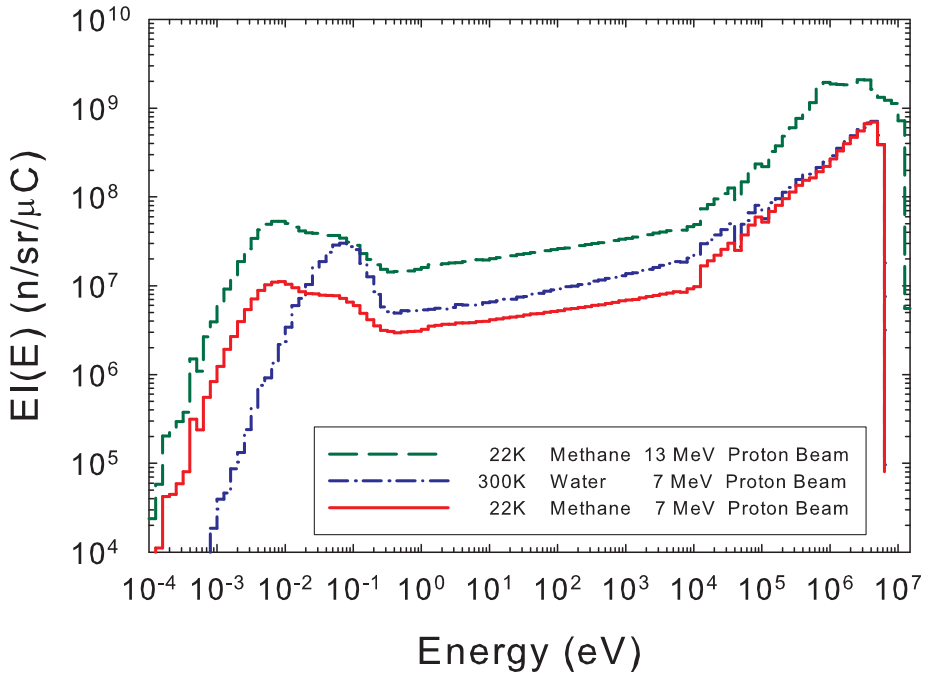

Figure 10. Neutron spectral intensity predicted by MCNP for different proton beam energies and TMR configurations. The discontinuity at 10 keV is due to the fact that the finite probability distribution used to model the primary neutron flux is not defined below this energy. As discussed later, the finite slope at epithermal energies may be associated with thin regions of the reflector around the cold moderator (see also fig. 15.)

where $C(t)$ is the count rate in the detector at time t after the start of the proton bombardment of the target, A is the area of the neutron beam on the detector, ΔT is the time channel width, and $\phi(E)$ is the neutron flux at the detector. We used a thin ^{3}He detector manufactured by LND [58]. The detector efficiency is determined by the pressure and thickness of the ^{3}He absorber:

$$\varepsilon(E) = 1 - e^{-n\sigma\frac{\lambda}{\lambda_o}x} = 1 - e^{-k\lambda} \tag{6}$$

where n is the number density of the neutron absorber, x is the absorber thickness, λ is the neutron wavelength wavelength, and σ is the absorption cross-section specified at λ_o. Efficiency is linear in wavelength when the detector is "thin", i.e. $k\lambda \ll 1$.

$$\varepsilon(E) \sim k\lambda \tag{7}$$

At LENS the simple relation between neutron energy and t is blurred by the long neutron emission time of the coupled moderator and the long width of the proton pulses. To completely account for this effect on the spectra, it would be

necessary to deconvolve the energy-dependent neutron pulse shape from the measured data. For simple spectral measurements, the dominant contribution to this correction can be accounted for by introducing an average delay from the start of the proton pulse to the first emission of neutron of a given energy from the moderator face. We therefore follow Ikeda and Carpenter [56] and define an average emission time delay, $\bar{t}(t)$. The dependence of this quantity on neutron energy is reflected in a dependence on arrival time at the detector, t. This emission time delay is required to determine the correct mean neutron energy in a TOF channel, $< E(t) >$, as shown in equation 8.

$$< E(t) >= \frac{1}{2} m (\frac{L}{t - \bar{t}(t)})^2 \tag{8}$$

This correction is typically small at a SPSS where $v\bar{t}$ is a small fraction of the flight path. At LENS, however, this correction is large for thermal neutrons: $v\bar{t}$ is ~ 90 cm for 200 meV neutrons, and ~ 50 cm for 10 meV neutrons, both of which are significant fractions of the 570 cm flight path. This is reflected in Figure 12, where the uncorrected data deviates from the corrected data for energies > 30 meV.

We use MCNP simulations to determine the mean energy in a TOF channel by calculating the integrals in Equation 9.

$$< E(t_i) >= \frac{\int_{t_{i-1}}^{t_i} dt \int_0^\infty dE \varepsilon(E) E \phi(E,t)}{\int_{t_{i-1}}^{t_i} dt \int_0^\infty dE \varepsilon(E) \phi(E,t)} \tag{9}$$

where t_i is the i^{th} time channel upper bound, and ε is the detector efficiency, which in this case is given by the cross-section for the ^{3}He(n,p) reaction. $< E(t) >$ is calculated at the position at which spectra are taken in the measurement, and $\Delta T = t_i - t_{i-1}$ is chosen to reflect the 100 μs channel width employed in the experiment. This may then in turn be used in Equation 8 to find $\bar{t}(t)$. The final result for $\bar{t}$ is shown in Figure 11 as a function of t.

3.2.3 Detector Efficiency Calibration

The absolute neutron flux was measured using the technique of gold-foil activation. Both bare and cadmium-covered gold foils were activated at the detector position simultaneously with the spectral measurements to provide an absolute calibration of the neutron detector efficiency [59,57]. The reason for employing cadmium in this type of measurement is easy to understand. Due to a low-lying resonance in ^{113}Cd, the transmission through a Cd foil is essentially a step function with a cutoff around 550 meV. Subtracting the Cd-covered activity from the activity of a bare foil allows one to reduce the impact on the

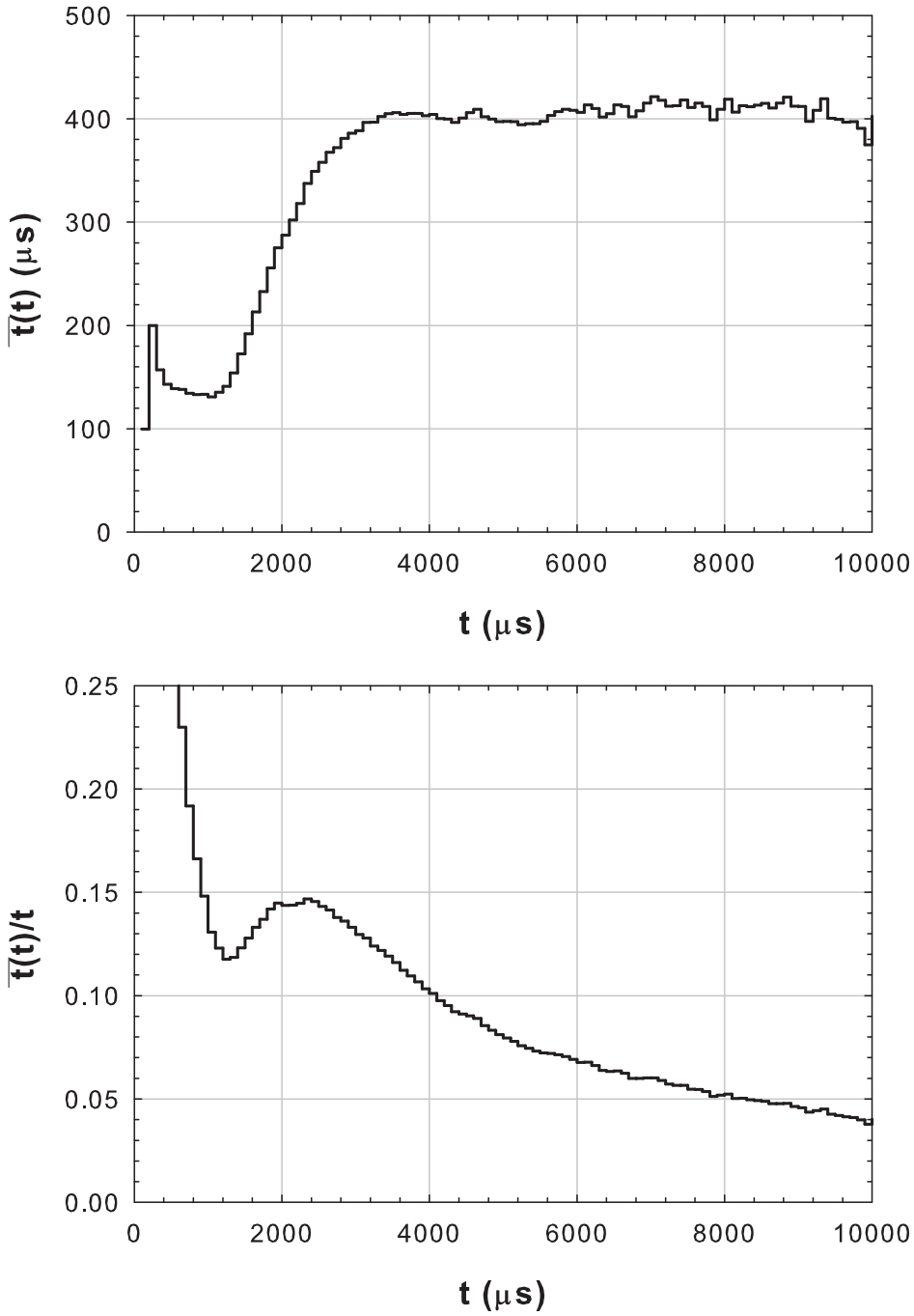

Figure 11. The simulated average emission time delay, $\bar{t}(t)$ from 22 K methane moderator. t is the time elapsed after the start of the proton pulse. The simulations use a 150 μs proton pulse and calculate the flux at a point 570 cm from the moderator, 20 degrees to the moderator normal. Note the delay can be as much as 15% of the time of flight for energies less than 50 meV.

activation per unit volume of the bare gold foil, $\tilde{A}_{bare}$, from that higher energy part of the spectrum which is not easily measured in the TOF experiment.

The saturation activities for the two gold foil measurements may then be related to the flux through the relations [60,61]:

$$\tilde{A} = \tilde{A}_{bare} - \tilde{A}_{cd} = \int_0^\infty dE\sigma(E)\Delta_{Cd}(E)\phi(E) \tag{10}$$

Where we have for cadmium absorption:

$$\Delta_{Cd}(E) = 1 - e^{-\Sigma_{cd}(E)x} \tag{11}$$

The foil activity was measured with a $\beta - \gamma$ coincidence method that allows absolute activity to be measured and absolute efficiencies for the gamma and electron detectors to be determined without a need for independent standard sources to provide the calibration [62]. The foils were placed between a lithium-drifted germanium detector, used for γ detection, and a plastic scintillator coupled to a photo-multiplier tube used as the β detector.

The apparatus was tested using a Au test foil activated closer to the source, the activity of which was measured periodically during a $\sim$2 week decay period from an original activity of about 100 Bq to a final activity below 1 Bq. The estimated uncertainties throughout the measurement, which increase as the foil decays, were consistent with the spread of the points around the average, and also consistent when evaluated against more precise measurements taken on other foils at even higher activities. At the lower activities, the uncertainty has significant contributions from both counting statistics and uncertainty in the background count rates. The measurements were performed at a facility with an operating 200 MeV cyclotron, and backgrounds were found to vary by 3 to 5% depending on the state of that accelerator. Therefore, as an added precaution, measurements were taken in five-minute time bins which were histogrammed and examined as a function of time to check for any anomalous readings or inconsistent trends in count rate before they were summed. For measurements with the foils in this study, no such anomalies were seen. The γ background signal in the β detector was measured using aluminum filters and a similar high-activity gold foil. With such an arrangement, the absolute efficiencies were determined to be about 4% in γ detection and about 13% in β detection.

At the end of the 10 hour irradiation at the sample position, the bare foil had activity of 3.7 Bq and the cadmium covered foil had activity of 1.0 Bq. The uncertainty in the absolute activity is approximately 12% for the bare foil using the coincidence counting method. This uncertainty estimate is in good

agreement with the differences between the activities calculated independently using the absolute gamma and beta detector efficiencies.

These data are used to determine a detector efficiency in the following manner. The data are converted to the energy domain using Equation 5 with the $\bar{t}$ correction for the energy. Then the unnormalized flux is weighted with the activation cross-section and the product integrated up to the maximum energy that can be measured with TOF to determine k. The proton pulse terminates at $150\mu s$, so the highest energy that can be reliably measured via TOF is about 2 eV. To perform the integration over the high energy regime we use a modified $\frac{1}{E^{1+\alpha}}$ slowing-down energy dependence to extrapolate to energies where the measured spectrum is unavailable. The leakage exponent, α, which accounts for deviation from the 1/E behavior due to losses through the boundaries of a finite moderating volume [11], is determined from a fit over that part of the epithermal spectrum that was measured.

The flux used in the numerical integration of Equation 10 is described by:

$$\begin{aligned}\phi(E) &= \phi_{th}(E) = \frac{C(t)}{\Delta T A \lambda \frac{dE}{dt}} \quad E < E_{max} \\ &= \phi_{epi}(E) = \phi_s \frac{1}{E^{1+\alpha}} \quad E_{max} < E < 5.2MeV \\ &= 0 \quad E > 5.2MeV \end{aligned} \tag{12}$$

Where ϕ_s is a constant related to the magnitude of the total epithermal flux chosen such that the flux is a continuous function of energy, ΔT is the TOF bin width, and A is the sample area. The cadmium total cross-section and gold (n,γ) cross-section were obtained from the ENDF/B-VI data set maintained by the Los Alamos Nuclear Data Service [63].

The absolute value of k for a low efficiency detector may then be related to the integrated activity through:

$$k = \frac{1}{\tilde{A}} \left(\int_0^{1eV} dE \sigma(E) \Delta_{Cd}(E) \phi_{th}(E) + \int_{1eV}^{5.2MeV} dE \sigma(E) \Delta_{Cd}(E) \phi_{epi}(E) \right) \tag{13}$$

We found that the second integral contributes 10% to the determination of k for $E_{max} = 1$ eV. This second term represents a correction for the finite absorption of neutrons by Cd at energies above the cut-off energy (note that this contribution goes to zero if the Cd absorbed no neutrons above 1 eV). The resulting value of k is $(4.40 \pm 0.88) \times 10^{-4}\, \mathring{A}^{-1}$ with the uncertainty dominated by that of the gold foil activity measurements.

The detector was specified to have an ideal efficiency of $5.47 \times 10^{-4}\, \mathring{A}^{-1}$ (1.91

cm thick, 3 Torr ^{3}He with 719 Torr ^{4}He as a buffer gas and 38 Torr N_2 as a quench gas). Uncertainties in the measured gas pressures are 0.1 Torr. The absolute efficiency determined from our gold-foil normalization is consistent with our specification to the manufacturer and also with an independent comparison of this detector to a calibrated detector via simultaneous measurement of the neutron spectrum on the HRMECS instrument at IPNS [59,64].

3.2.4 Measured Neutron Energy Spectra

The collimation used to assure that the measurement looked only at neutrons emitted from the moderator face consisted of two 20 cm long steel collimators combined with 0.635 cm thick boron nitride (BN) masks upstream of the first collimator and downstream from the second. The collimator diameters are 7.62 cm at a distance of 140 cm from the moderator face and 2.54 cm at a distance of 570 cm. To facilitate rapid measurement of spectra at different moderator temperatures we used a high efficiency (black) LND 25291 neutron detector containing 20 ATM of ^{3}He that was masked by an additional BN aperture of roughly 3 mm diameter to reduce dead time effects from high instantaneous count rates at short wavelengths. To calibrate this detector, the 4 K spectrum collected with it was fitted to an equivalent spectrum taken with the thin detector with one free parameter to account for uncertainty in the precise dimensions of the small aperture in front of the thick detector. The RMS differences between the neutron spectra measured by the two detectors between 18 and 1000 meV was only 2.5%. The empty moderator and 4 K methane spectra (shown in figs. 12 and 13) were taken with the thin detector, and the 25 K spectrum was taken with the black detector (fig. 13).

Tables 3 and 4 show integrated neutron yields for various neutron energy groups and the "1 eV coupling" for an empty moderator vessel (water reflector moderated neutrons) and solid methane moderator. The 1 eV coupling is the value of spectral intensity (EI(E)) evaluated at 1 eV, and for a 1/E spectrum it is proportional to the epithermal neutron flux [11,59]. For this reason it is a common benchmark used for discussing the performance of a moderator system. For the empty moderator, the measured integrated neutron yields below 125 meV agree remarkably well with the simulation once the correction for the emission time delay is applied, as shown in Figure 12. With an empty moderator vessel, the neutron spectrum depends almost exclusively on the water reflector, for which the scattering kernels have been well characterized. The dominant contribution to the 25% uncertainty in these measurements is the absolute efficiency of the detector, with additional contributions coming from proton current normalization and background determination.

The methane moderator was prepared by liquifying pure methane from the gaseous state in the moderator vessel. The methane was then cooled from liq-

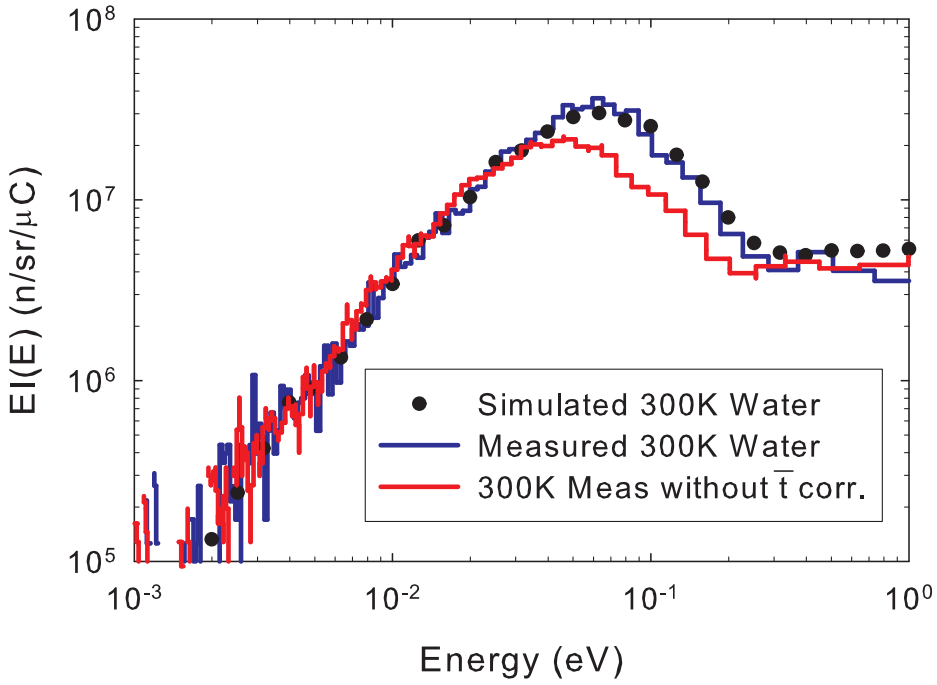

Figure 12. The water moderated spectral intensity, with and without the $\bar{t}$ correction applied to the data compared to simulation.

uid to the 4 K base temperature in about 2 hours. Cold moderator neutron energy spectra were measured using the high efficiency neutron detector during the moderator cool-down in order to obtain spectral information in short exposure times. Once the moderator reached 4 K, the flux was also measured both with the black detector and using gold foil activation together with the 1/v detector (as described in Section 3.2.3).

When the moderator is filled with solid methane the measured 1 eV coupling agrees within the experimental uncertainty with the MCNP simulations, but agreement with the simulated integrated yields is not as satisfying (Figure 13 and Table 4). The spectral differences between simulation and measurement we see below 100 meV may be related to inadequacies in the existing scattering kernel for methane, or it could be related to defects in the methane introduced by our method of preparation. Measurements of solid methane by Grieger et al. have shown that rapid solidification can introduce inhomogeneities large enough to affect the total neutron cross-section [47]. The cross-section is also known to be sensitive to the total spin state of the identical protons in the methane molecule, which we did not control in these measurements. The *smeth22K* kernel is based upon a phonon expansion with 4 discrete modes to model the excitations of the hydrogen about the central carbon atom. Two recently-developed approximate theories exist for the dynamic structure factor of solid methane which include the contribution from hindered rotors and

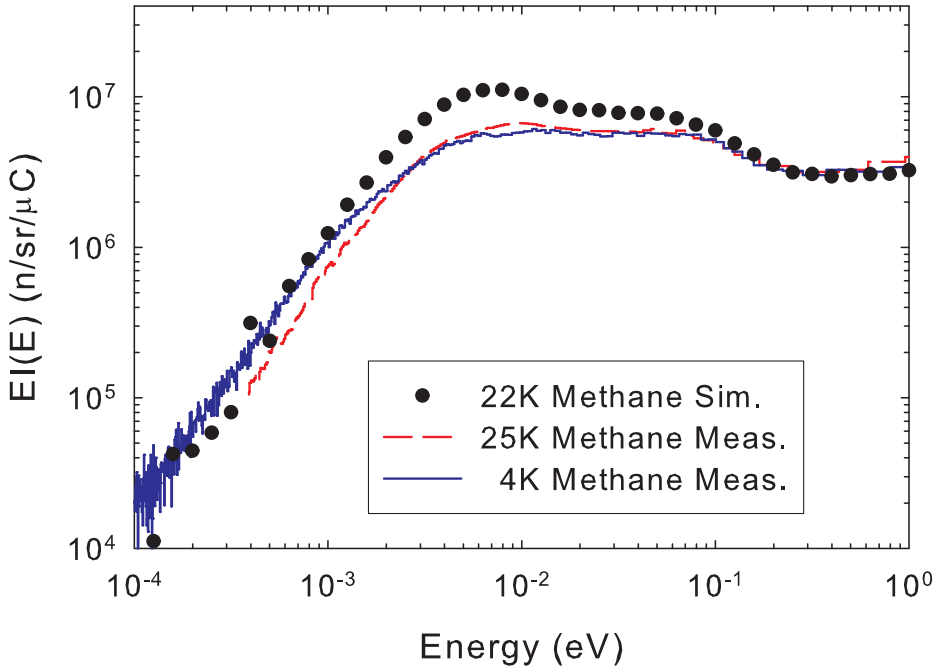

Figure 13. $EI(E)$ for solid methane at 25 K and 4 K temperatures as a function of neutron energy.

Table 3
Empty Moderator Vessel: Table of experimental and simulated integral neutron yields from the LENS TMR operated with a 7 MeV proton beam and a 150μs wide proton pulse. Units of $10^6 n/sr/\mu C$.

Energy Group (meV)	**MCNP**	**Meas.**
0.20-0.82	0.0091 ± 0.0005	< 0.04
0.82-3.27	0.304 ± 0.001	0.22 ± 0.05
3.27-10	1.72 ± 0.01	1.64 ± 0.37
10-125	44.30 ± 0.07	47.6 ± 10.6
1 eV Coupling	5.35 ± 0.09	3.8 ± 0.9

correctly account for the spin state of the methane molecules in the phase II crystal structure that is present below 20 K [65,45,66]. Comparison of spectra from moderators condensed under a variety of conditions to predictions from these recently developed kernels will be the subject of a future publication.

Table 4
Solid Methane Moderator: Table of experimental and simulated integral neutron yields for 7 MeV proton beam, 150μs wide proton pulse. Units of $10^6 n/sr/\mu C$.

Energy Group (meV)	**22K MCNP**	**25K Meas.**	**4K Meas.**
0.20-0.82	$0.463 \pm .002$	0.18 ± 0.04	0.44 ± 0.09
0.82-3.27	6.37 ± 0.02	2.4 ± 0.5	3.3 ± 0.7
3.27-10	$10.40 \pm .01$	6.3 ± 1.2	6.2 ± 1.3
10-125	19.05 ± 0.01	14.1 ± 2.8	13.2 ± 2.7
1 eV Coupling	$3.25 \pm .02$	3.5 ± 0.7	4.0 ± 0.8

4 Possible Improvements to Cold Neutron Brightness through Design Modifications

There are a number of modifications to the design of the LENS TMR that could increase the cold neutron brightness from the moderator. The present design uses an oversized vacuum space around the moderator to facilitate experiments on a variety of moderator choices during our initial low-power operation. To investigate the impact of this extra vacuum space on the neutronic performance, the size of the vacuum gaps was varied in the MCNP model. The cold leakage flux between 0 and 10 meV from the moderator was simulated as a function of the water layer thickness between the target and moderator for a number of values for the vacuum space dimensions below, and to the sides of the moderator. The results of these simulations are shown in Figures 14 and 15. Up to a 30% increase in the leakage flux below 10 meV is possible simply by reducing the size of the vacuum gaps. We also notice that decreasing the size of these vacuum spaces also brings the spectrum from 1 eV to 10 keV closer to the 1/E behavior expected for an infinite moderator [11]. Figure 15 therefore suggests that some of the gain seen here may come from avoiding under-moderation in thin sections of the reflector as well as from bringing reflector material closer to the moderator itself.

Another potential gain for the neutron flux available at LENS may be obtained by changing to a beryllium reflector. Calculations indicate an increase in the brightness of an additional 30% without a significant increase in the width of the emission time distribution is possible. The expense and potential for activation due to impurities in the Be have precluded us from implementing this option in the initial construction of the facility. The smaller absorption cross section and less efficient moderation associated with n-Be collisions (compared to n-H) require a slightly larger Be reflector volume. The present water reflector was sized with this potential upgrade in mind so it could be implemented with essentially no impact on the other components of the TMR. It is also possible that a Be reflector/filter covering the instrument beam lines

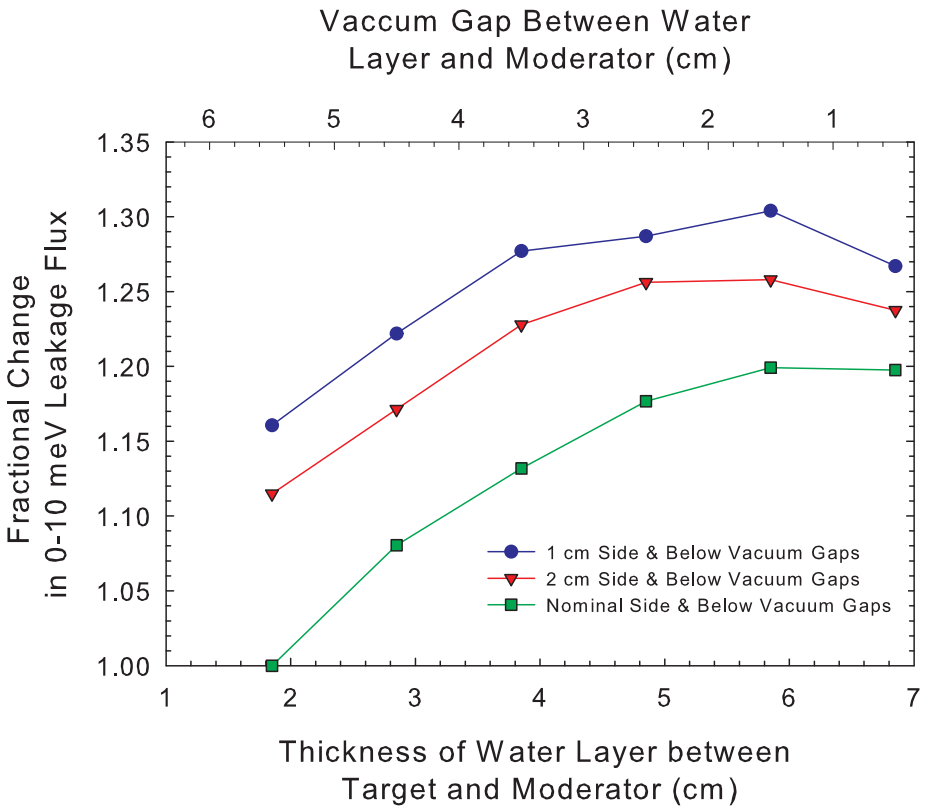

Figure 14. A simulation of the cold leakage flux enhancement expected from increasing the thickness of reflector material between the target and moderator. The enhancement is greater if voids along the sides and below the moderator are reduced to 1 cm from the moderator vessel surface.

could achieve similar gains in flux while requiring much less Be [67]. In this configuration, cold Be directly in front of the moderator is used to reflect epithermal neutrons back while transmitting neutrons with energies below the Bragg cutoff to the instruments.

Finally, MCNP simulations with a recently developed kernel for solid methane [65] suggest that increasing the moderator thickness to 2 cm will increase the cold-neutron brightness and reduce the spectral temperature. As a first step to check on this possibility we will investigate the effect of inserting a cold polyethylene premoderator on the thermal shield in the cryogenics system. This has the advantage of reducing the thermal and radiation loads on the moderator (as opposed to the increase in these that would accompany an increase in the methane thickness itself) while still providing extra material behind the moderator's front face to cool neutrons below room temperature. A major goal for the facility over the next several years is to develop moderator materials and designs suitable for reducing the spectral temperature of the moderator, and this will be but the first step in that on-going effort. Enhancements in moderator geometry, such as grooved and reentrant cavity type moderator will also be explored in simulation to assess their ability to

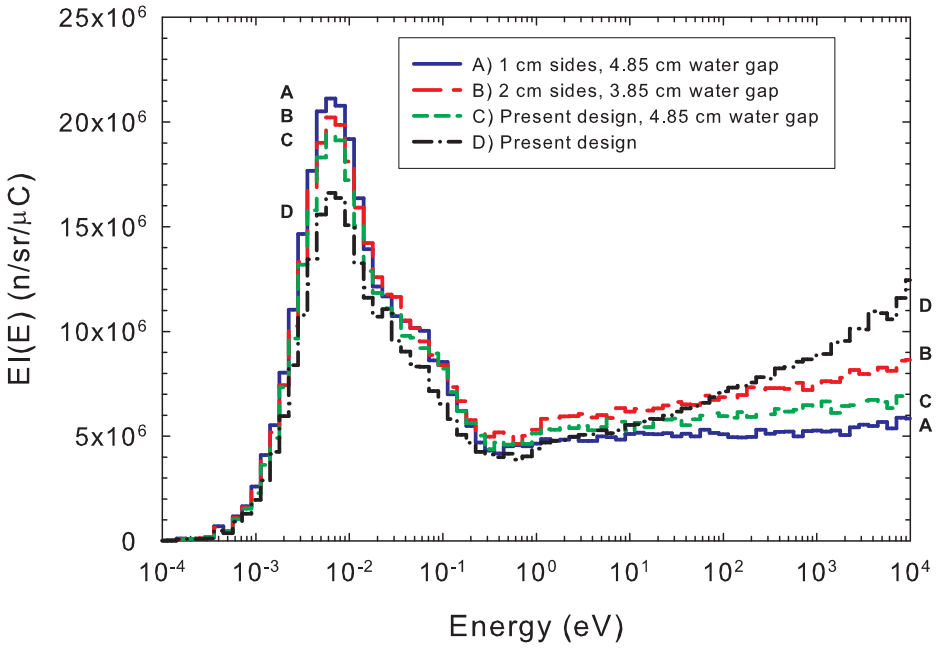

Figure 15. Simulations of neutron energy spectra for representative configurations from Figure 14 show the impact of water premoderator layer thickness and vacuum gap thickness on cold neutron leakage flux. The optimal Case (A) minimizes vacuum gaps and optimizes premoderator thickness. Case (B) has less cold flux than Case (A) due to enlarged side gaps. Case (C) is similar, where present design's current side gap thickness is unchanged and premoderator layer alone is optimized. Case (D) is the present design, where the high leakage from the TMR causes the slope of the 1-10^4 eV flux to increase while at the same time reducing coupling between the moderator and reflector.

improve cold neutron yield.

5 Conclusion

In this paper we have described the modular design approach taken for the LENS neutron source and explained the simple physical considerations which set the scale for the dimensions of the target/moderator/reflector system and timescales for the time-dependent neutron field from this strongly-coupled long pulse neutron source. We have discussed in detail all design features relevant for neutron production and moderation. We have also outlined the assumptions of our MCNP model for LENS and compared the measured brightness, energy spectrum, intensity, and emission time distribution with MCNP predictions, which agree within the accuracy of the measurements and the uncertainly of the actual neutronic properties of the moderator.

We hope that this description of the design of LENS will be useful in the future for those readers who choose to construct their own neutron source. The LENS operating regime opens up some interesting possibilities for different types of neutron sources which have not been fully investigated.

Acknowledgements

The authors would like to thank P. D. Ferguson and E.B. Iverson for many helpful discussions. We are also grateful to J.M. Carpenter for the loan of the equipment used at the Intense Pulsed Neutron Source (IPNS) in reference [56] for the emission time measurements. Computational work was supported by Shared University Research grants from IBM, Inc. to Indiana University and by the National Science Foundation under Grant No. 0116050. The LENS project is supported by the National Science Foundation (under grants DMR-0220560 and DMR-0320627), the Indiana 21st Century Fund, Indiana University, and Crane Naval Surface Warfare Center.

M. Snow thanks the Institute for Nuclear Theory at the University of Washington for its hospitality and the Department of Energy for partial support during the completion of this work.

References

[1] D. V. Baxter, J. M. Cameron, V. P. Derenchuk, C. M. Lavelle, M. B. Leuschner, M. A. Lone, H. O. Meyer, T. Rinckel, W. M. Snow, NIM B 241 (2005) 209–212.

[2] D. V. Baxter, A. Bogdanov, J. M. Cameron, P. Chen, V. P. Derenchuk, B. Jones, H. Kaiser, C. M. Lavelle, M. B. Leuschner, M. A. Lone, H. O. Meyer, H. Nann, N. Remmes, T. Rinckel, W. M. Snow, P. E. Sokol, in: G. Russell, J. Rhyne, B. V. Maes (Eds.), ICANS-XVII, Vol. I, Los Alamos Neutron Science Center, Santa Fe, New Mexico, 2005, pp. 18–24.

[3] F. Mezei, Physica B 234-236 (1997) 1227–1232.

[4] J. Stride, D. Wechsler, F. Mezei, et al., Nucl. Instr. Methods A 451 (2003) 480–491.

[5] F. Mezei, M. Russina, S. Schorr, Physica B 276 (2000) 181–182.

[6] G. H. Lander, J. M. Carpenter, Physica B+C 137 (1-3) (1986) 373–378.

[7] G. Muhrer, E. J. Pitcher, G. J. Russell, T. Ino, M. Ooi, Y. Kiyanagi, NIM A 527 (3) (2004) 531–542.

[8] T. E. Mason, D. Abernathy, I. Anderson, J. Ankner, T. Egami, G. Ehlers, A. Ekkebus, G. Granroth, M. Hagen, K. Herwig, J. Hodges, C. Hoffmann, C. Horak, L. Horton, F. Klose, J. Larese, A. Mesecar, D. Myles, J. Neuefeind, M. Ohl, C. Tulk, X. L. Wang, J. Zhao, Physica B: Condensed Matter 385-386 (Part 2) (2006) 955–960.

[9] D. J. Picton, S. M. Bennington, T. A. Broome, T. D. Beynon, Nuclear Instruments and Methods in Physics Research Section A: Accelerators, Spectrometers, Detectors and Associated Equipment 545 (1-2) (2005) 363–374.

[10] M. Harada, N. Watanabe, M. Teshigawara, T. Kai, Y. Ikeda, NIM A 539 (1-2) (2005) 345–362.

[11] J. M. Carpenter, W. Yelon, Methods of Experimental Physics, Volume 23: Neutron scattering; Part A, Chap. 2, Academic Press, Orlando, 1986.

[12] C. G. Windsor, Pulsed Neutron Scattering, Taylor and Francis, New York, 1981.

[13] N. Watanabe, Rep. Prog. Phys. 66 (2003) 339–381.

[14] B. J. Micklich, J. M. Carpenter (Eds.), Proceedings of the Workshop on the Applications of a Very Cold Neutron Source, Argonne National Laboratory report ANL-05/42, 2005.

[15] R. Golub, Rev. Mod. Phys. 68 (1996) 329–347.

[16] X-5 Monte Carlo Team, MCNP-A General Monte Carlo N-Particle Transport Code, Version 5 Volume II: Users Guide, Tech. Rep. LA-CP-03-0245, Los Alamos National Laboratory (2003).

[17] S. Glasstone, M. C. Edlund, The elements of nuclear reactor theory, Van Nostrand, New York,, 1952.

[18] M. M. R. Williams, The Slowing Down and Thermalization of Neutrons, North-Holland Pub. Co., Amsterdam, 1966.

[19] A. V. Klyachko, V. P. Derenchuk, A. A. Bogdanov, K. Solberg, Review of Scientific Instruments 77 (3) (2006) 03B501.

[20] V. Derenchuk, D. Baxter, A. Bogdanov, W. Jones, T. Rinckel, K. A. Solberg, in: 2005 Particle Accelerator Conference, Knoxville, Tennessee, 2005, pp. 3200–3202.

[21] V. Derenchuk, D. Baxter, A. Bogdanov, W. Jones, A. Klyachko, T. Rinckel, P. Sokol, K. Solberg, in: LINAC 2006, Knoxville, TN, 2006.

[22] D. L. Friesel, W. Hunt, in: XIX International Linac Conference, Chicago, IL, 1998, pp. 61–63.

[23] J. Guzek, W. R. McMurray, T. Mateva, C. B. Franklyn, U. A. S. Tapper, NIM B 139 (1-4) (1998) 471–475.

[24] R. W. Peelle, F. C. Maienschein, Physical Review C 3 (1) (1971) 373.

[25] F. Pleasonton, R. L. Ferguson, H. W. Schmitt, Physical Review C 6 (3) (1972) 1023.

[26] V. V. Verbinski, H. Weber, R. E. Sund, Physical Review C 7 (3) (1973) 1173.

[27] Y. Kiyanagi, S. Satoh, H. Iwasa, F. Hiraga, N. Watanabe, Physica B 213-214 (1995) 857–859.

[28] M. Oi, Y. Kiyanagi, J. Nuc. Sci and Tech 41 (1) (2004) 15–20.

[29] K. Inoue, Y. Kiyanagi, H. Iwasa, NIM 192 (1982) 129–136.

[30] J. M. Carpenter, Nature 330 (6146) (1987) 358–360.

[31] E. Kulagin, S. Kulikov, V. Melikhov, E. Shabalin, NIM B 215 (1-2) (2004) 181–186.

[32] Technical concepts for a long-wavelength target station for the spallation neutron source. anl-02/16, ornl/sns-tm-2001/163, 2002.

[33] J. K. Shultis, R. E. Faw, Radiation shielding, American Nuclear Society, La Grange Park, IL, 2000.

[34] Borated FLex Panel 227A from Thermo Electron Corp. Los Altos CA, 94024.

[35] NCRP Report No. 38, Protection Against Neutron Radiation. Appendix E., 1965.

[36] P. Chen, W. Wu, B. G. Jones, T. A. Newell, in: 2006 Internation Congress on Advances in Nuclear Power Plants (ICAPP '06), Reno, NV, 2006.

[37] M. A. Lone, C. B. Bigham, J. S. Fraser, H. R. Schneider, T. K. Alexander, A. J. Ferguson, A. B. Mcdonald, NIM 143 (2) (1977) 331–344.

[38] M. A. Lone, in: S. M. Qaim (Ed.), Proceedings of the Int'l Conf. on Nuclear Data for Science and Technology OECD Nuclear Energy Agency, IAEA, Springer Verlag, Berlin, 1992, p. 678.

[39] H. J. Brede, G. Dietze, K. Kudo, U. J. Schrewe, F. Tancu, C. Wen, NIM A 274 (1-2) (1989) 332–344.

[40] W. B. Howard, S. M. Grimes, T. N. Massey, S. I. Al-Quraishi, D. K. Jacobs, C. E. Brient, J. C. Yanch, Nuclear Science and Engineering 138 (2) (2001) 145–160.

[41] H. Nann, unpublished (2006).

[42] R. C. Byrd, C. E. Floyd, K. Murphy, R. L. Walter, Nucl. Phys A399 (1983) 94.

[43] DROSG-2000: Neutron Source Reactions, IAEA-NDS-87, 1987.

[44] P. G. Young, A. E. D., M. Bozian, E. T. R., G. M. Hale, R. J. LaBauve, R. C. Little, Los Alamos National Laboratory Report LA-11753-MS (1990) 1.

[45] F. Cantargi, J. R. Granada, S. Petriw, M. M. Sbaffoni, Physica B: Condensed Matter 385-386 (Part 2) (2006) 1312–1314.

[46] R. E. MacFarlane, in: J. M. Carpenter, E. Iverson (Eds.), International Workshop on Cold Moderators for Pulsed Neutron Sources, OECD OCDE, Argonne National Laboratory, 1997, pp. 221–231.

[47] S. Grieger, H. Fridrich, K. Guckelsberger, R. Scherm, W. Press, J. Chem. Phys. 109 (8) (1998) 3161–3175.

[48] Y. Shin, W. M. Snow, C. Lavelle, D. V. Baxter, M. Leuschner, W. Lozowski, H. Nann, N. Remmes, T. Rinckel, P. E. Sokol, in: G. Russell, J. Rhyne, B. V. Maes (Eds.), ICANS-XVII, Vol. II, Los Alamos Neutron Science Center, Santa Fe, New Mexico, 2005, pp. 542–550.

[49] Y. Kiyanagi, N. Watanabe, H. Iwasa, NIM A 312 (1992) 561–570.

[50] Y. Kiyanagi, J. M. Carpenter, N. Kosugi, H. Iwasa, F. Hiraga, N. Watanabe, Physica B 213-214 (1995) 854–856.

[51] Cryomech, http://www.cryomech.com/.

[52] Pechiney World Trade Corp., Stamford, CT, 06902.

[53] A. Jezowski, H. Misiorek, V. V. Sumaroko, B. Y. Gorodilov, Phys. Rev. B 55 (1997) 5578–5580.

[54] J. M. Carpenter, A. W. Shulke, T. Scott, D. G. Wozniak, in: Proceedings of the Eighth Meeting of the International Collaboration on Advanced Neutron Sources (ICANS-VIII), Rutherford Appleton Labratory, Oxford, England, 1985, pp. 311–318.

[55] K. F. Graham, J. M. Carpenter, NIM 85 (1970) 163–171.

[56] S. Ikeda, J. M. Carpenter, NIM A 239 (1985) 536–544.

[57] E. B. Iverson, J. M. Carpenter, E. J. Hill, in: J. M. Carpenter, E. Iverson (Eds.), International Workshop on Cold Moderators for Pulsed Neutron Sources, OECD OCDE, Argonne National Laboratory, 1997, p. 191.

[58] LND, http://www.lndinc.com/.

[59] B. J. Micklich, E. B. Iverson, D. W. Freeman, R. G. Cooper, P. D. Ferguson, F. X. Gallmeier, S. E. Hammons, I. Popova, D. V. Baxter, C. M. Lavelle, in: G. Russell, J. Rhyne, B. V. Maes (Eds.), ICANS-XVII, Vol. II, Los Alamos Neutron Science Center, Santa Fe, New Mexico, 2005, pp. 463–472.

[60] G. F. Knoll, Radiation detection and measurement, 2nd Edition, Wiley, New York, 1989.

[61] Annual Book of ASTM Standards, Vol. 12, ASTM International, 2003.

[62] V. G. Wolf, Nukleonick 2 (7) (1961) 255–271.

[63] Los Alamos Nuclear Data Service, http://www.cryomech.com/.

[64] E. B. Iverson, B. J. Micklich, D. V. Baxter, R. G. Cooper, P. D. Ferguson, D. W. Freeman, F. X. Gallmeier, S. E. Hammons, C. M. Lavelle, I. Popova, in: G. Russell, J. Rhyne (Eds.), ICANS-XVII, Vol. II, Los Alamos, Santa-Fe, 2005, pp. 436–446.

[65] Y. Shin, W. M. Snow, C. Lavelle, D. V. Baxter, et. al, to be submitted to Phys. Rev. B.

[66] S. Petriw, F. Cantargi, J. R. Granada, M. M. Sbaffoni, O. Lovotti, Physica B: Condensed Matter 385-386 (Part 2) (2006) 1309–1311.

[67] G. Muhrer, E. J. Pitcher, G. J. Russel, in: G. Russell, J. Rhyne, B. V. Maes (Eds.), ICANS-XVII, Vol. II, Los Alamos Neutron Science Center, Santa Fe, New Mexico, 2005, pp. 678–688.